Materials Today Energy 16 (2020) 100374

Contents lists available at ScienceDirect

Materials Today Energy

journal homepage: www.journals.elsevier.com/materials-today-energy/

AC/Se composite cathode for asymmetric Li-ion capacitors

Yiyong Zhang [a], Mingsheng Xu [b], Huaicong Yan [a], Qi Meng [a], Xue Li [a], Peng Dong [a], Yingjie Zhang [a, **], Jinbao Zhao [b, *]

[a] National and Local Joint Engineering Laboratory for Lithium-ion Batteries and Materials Preparation Technology, Key Laboratory of Advanced Battery Materials of Yunnan Province, Faculty of Metallurgical and Energy Engineering, Kunming University of Science and Technology, Kunming, 650093, PR China

[b] State Key Laboratory of Physical Chemistry of Solid Surfaces, State-Province Joint Engineering Laboratory of Power Source Technology for New Energy Vehicle, Collaborative Innovation Center of Chemistry for Energy Materials, College of Chemistry and Chemical Engineering, Xiamen University, Xiamen, 361005, PR China

ARTICLE INFO

Article history:
Received 29 July 2019
Received in revised form
27 November 2019
Accepted 9 December 2019
Available online xxx

Keywords:
Lithium-selenium asymmetric capacitor
Activated carbon-selenium cathode
Pre-lithiated graphite anode

ABSTRACT

The asymmetric capacitors are one of the energy storage systems that provide high energy density and high power density. However, there are some limitations which impede the development of asymmetric capacitors. In this context, we designed a new type of lithium-selenium asymmetric capacitor (LSEC) that has both the capacitive effect and the diffusion-controlled reaction. The LSECs use the activated carbon-selenium (AC-Se) as a mixed cathode material and the pre-lithiated graphite as an anode material which can exhibit the electrochemical reduction/oxidation of Se and the adsorption/desorption of anions at substantially the same rate. This novel LSEC solves the problem of imbalance between the energy and the dynamics, and provides a solution to provide both high energy density and high power density, thus has great application potential.

1. Introduction

Human beings are facing with problems such as depletion of resources, serious environmental pollution, and climate change caused by the consumption of fossil fuels. An effective technique to solve these problems is to develop new renewable and sustainable energy systems. Nowadays, solar energy, tidal energy and wind power have been used increasingly in recent decades, and the electric vehicles with low carbon dioxide emissions have been promoted. However, the use of these renewable energy sources is constrained by geography, climate and time. Therefore, in order to realize an effectively utilization of renewable energy, it is imperative to develop a low cost and environmentally friendly energy storage system with good safety and high performance. The lithium-ion batteries (LIBs) and the super-capacitors have been considered as good choices for the development in these energy storage systems [1–5]. Unfortunately, despite the commercialization of LIBs, they are unable to meet the high power requirements of applications for large electrical tools, electric vehicles, and high-efficiency storage devices for renewable energy. Compared to traditional dielectric capacitors, the super-capacitors not only offer the potential for the high power systems, but also provide higher energy densities, since they provide a higher power density than the LIBs in an instant. However, the energy density of traditional super-capacitors is still insufficient to meet the requirement of high energy and high power density for new applications. Apparently, both the energy and power densities of each energy storage system must be enhanced to satisfy such new application requirement [6–8].

In order to overcome these disadvantages, recent researches on LIBs have concentrated on improving the electrode materials, for example, introducing high capacity silicon anodes and high capacity lithium-rich cathodes. However, these materials inherently have several drawbacks, including short cycle life, poor rate performance, low initial coulombic efficiency, unsatisfactory thermal characteristics, and severe voltage drop [9]. In fact, some alternative energy storage systems, such as lithium-sulfur batteries, lithium-air batteries, sodium-ion batteries and magnesium-ion batteries, have been proven to superior to LIBs in energy and power density, cost and safety. However, these new energy storage systems still suffer from some challenges [10–13]. Therefore, in order to solve these problems, a new type of asymmetric energy storage systems have recently been put forward, which can combine the high rate

---

* Corresponding author:
** Corresponding author:
E-mail addresses: zyjkmust@126.com (Y. Zhang), jbzhao@xmu.edu.cn (J. Zhao).

https://doi.org/10.1016/j.mtener.2019.100374

performance of super-capacitors with the high energy density of LIBs [14]. These asymmetric energy storage systems involve two different kinds of electrode materials, namely the faradaic redox LIB materials and the anion adsorption-desorption capacitor materials. So far, there are two key ways to obtain these asymmetric energy storage systems, one is pseudo capacitve capacitor and the other is lithium-ion capacitor(LIC). The working principle of LIC is lithium-ions intercalation/deintercalation in the electrode bulk combined with anions adsorbed/desorbed on the surface of the active carbon (AC) cathode [15,16]. Although the LICs based on AC-based cathodes and lithium-doped carbon anodes display higher energy densities and operating voltages than the super-capacitors, the unbalanced dynamics between the two electrodes must be addressed in order to achieve their commercial application. To address these key challenges, Roh's group has reported the construction of novel lithium-sulfur capacitors (LSCs) which can balance power and energy densities [17]. In their asymmetric LSCs, a prelithiated graphite electrode and AC/S composite electrode with small quantities of S were used as the anode and hybrid cathode, respectively, and they exhibited anion adsorption-desorption in addition to the electrochemical reduction and oxidation of S at almost identical rates between the prelithiated graphite anode and the AC/S cathode. Due to a high theoretical specific capacity of S (1675 mAh g^{-1}), the LSCs can overcome the low specific capacitance posed by conventional AC, and finally achieve a stable high capacity, excellent rate performance and good cycling efficiency. As a result, when using as advanced asymmetric energy storage systems, the LSCs undergo both faradaic and nonfaradaic reactions, thereby providing greater power densities than LIBs and higher energy densities than the super-capacitors.

To further develop this strategy, we herein report the use of Se instead of S to prepare the lithium-selenium asymmetric capacitors (LSECs) in accordance with the LSCs' design. In our system, a prelithiated graphite electrode and AC/Se composite electrode with small quantities of Se will be used as the anode and hybrid cathode, respectively, the LSCs undergo both faradaic and nonfaradaic reactions between the prelithiated graphite anode and the AC/Se cathode which can balance power and energy densities. Compared to S, the selenium (Se) has higher electronic conductivity and higher density, the effect of the same mass of Se on the pores and conductivity of AC is small. Therefore, Se can promote LSECs to achieve higher loading of active material, higher area capacity and higher rate property.

2. Experimental section

2.1. Material preparation

The AC/Se composite (AC-Se) was prepared using a melt-diffusion method. Specifically, the AC (Fuzhou Yihuan Carbon Co., Ltd., china) and Se powder (Sigma-Aldrich) were mixed and grinded at a mass ratio of 90:10, followed by heating in a vacuum glass tube at 260 °C for 3 h, and the obtained composite was labeled as AC-Se-10. At the same time, AC-Se composites were prepared in the same manner according to a mass ratio of AC: Se at 95:5 and 85:15, labeling as AC-Se-5 and AC-Se-15, respectively.

2.2. Materials characterizations

The scanning electron microscopy (SEM) images of as-prepared AC-Se composite and the AC were characterized using a scanning electron microscope (SEM, HITACHI S-4800) equipped with energy dispersive X-ray spectroscopy (EDX) for elemental analysis. Thermogravimetric (TG) analysis was performed on a SDTQ600. The dried sample of 5–10 mg was placed in an Al_2O_3 pan and heated from 35 °C to 800 °C at 10 °C min^{-1} under a flow of nitrogen atmosphere. The XRD patterns of AC-Se composite and AC were recorded by the Philips X'pert Pro Super X-ray diffractometer and Cu Kα radiation. The nitrogen adsorption-desorption isotherms were obtained at liquid nitrogen temperature by automatic physical and chemical adsorption equipment (ASAP2020HD88 + C, Micromeritics Instruments Corp).

2.3. Electrochemical characterizations

The cathode slurry was composed of 80 wt% AC-Se composite, 10 wt% Super-P (a commercial conductive carbon blacks) and 10 wt % polytetrafluoroethylene (PTFE) which was dissolved in deionized water, then the slurry was casted onto a stainless steel mesh and dried under vacuum at 60 °C overnight to prepare the mixed cathode. The areal load of the electrode was about 10 mg cm^{-2}. The anode was prepared by graphite electrode prior to connecting to a Li-metal foil. The slurry with a composition of 90 wt% graphite, 5 wt % Super-P and 5 wt% PTFE was casted onto a stainless steel mesh to prepare a graphite electrode. The CR2016-type coin cells were assembled using the prepared mixed cathode and anode in an argon-filled glove box. The volume of the electrolyte in a coin cell was 100 μL. The electrolyte was formed by adding lithium bis(trifluoromethanesulfonyl)imide (LiTFSI, 1 M) salt and lithium nitrate ($LiNO_3$, 1 wt%) into the mixture of 1,3-dioxolane (DOL) and 1,2-dimethoxyethane (DME) at a volume ratio of 1:1. The separator was polypropylene (Celgard 2400). The galvanostatic charge-discharge experiments were measured at different current densities between 1.5 and 3.8 V (vs. Li^+/Li) using a CT2001A cell test instrument (XINWEI Electronic Co.). The cyclic voltammogram (CV) curves were tested on the Autolab PGSTAT 101 cell in a voltage range between 1.5 V and 3.8 V (vs Li^+/Li), at a scan rate from 0.1 mV s^{-1} to 1.0 mV s^{-1}. The relevant LICs (the AC as the cathode material and the prelithiated graphite as the anode material in the capacitors) were also tested at the same current in the voltage range of 1.5–3.8 V. All of the electrochemical tests were performed at room temperature.

3. Results and discussion

The LSEC is a new class of asymmetric energy storage system which combines the high rate performance of super-capacitors with high energy density of lithium-Se batteries. These systems contain two different types of electrode materials, namely faradaic redox AC-Se materials and porous AC for super-capacitors. The LSECs can simultaneously exhibit the capacitive behavior of anion absorption/desorption and the electrochemical behavior of Se electrochemical redox, resulting in both high energy density and

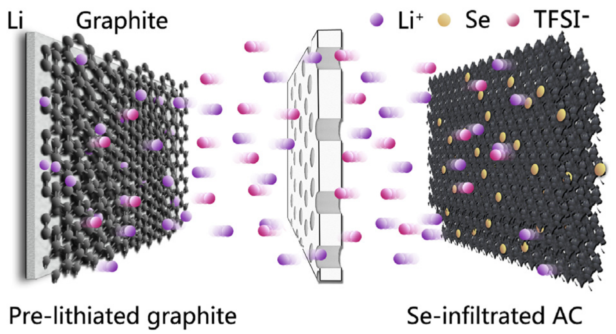

Scheme 1. Schematic of the LSECs showing the selectively Se-infiltrated AC (AC-Se) cathode and the prelithiated graphite anode.

high power density. As shown in Scheme 1, the LSECs are composed of a mixed cathode, a pre-lithiated anode, an electrolyte and a separator, wherein the mixed cathode active material is a composite material in which the Se is infiltrated in the porous AC. The pre-lithiated anode is formed by pressing a graphite anode on the surface of lithium metal. The electrolyte is an electrolyte for a lithium-sulfur battery, and the separator is a LIB separator.

The morphologies of AC and AC-Se composite and the corresponding EDX mappings for C and Se of AC-Se composite are shown in Fig. 1 and Fig. S1. The results show that there is almost no change in the morphology of AC after the infiltration of Se into AC to form AC-Se composite. The element mapping result of AC-Se composite (Fig. 1e and Fig. S1c and S1d) confirms that the Se is uniformly distributed in the AC.

In order to determine the crystal structure and the amount of Se in AC-Se composite, the XRD and TG tests have been carried out, and the results are shown in Fig. 2a, b and Fig. S2 and S3. According to Fig. 2a, and Fig. S2, the XRD patterns of AC-Se composite and AC are identical, and no characteristic peaks of Se are found in the AC-Se composite. This further illustrates that the Se is uniformly distributed in the AC. Meanwhile, it can be seen from Fig. 2b and Fig. S3 that the content of Se in the AC-Se-5, AC-Se-10 and AC-Se-15 are 4.0%, 7.1% and 12.4%, respectively. According to the TG curve, the loss cut-off temperature of Se in the AC-Se-10 (about 400 °C) is higher than that of Se, indicating the strong interaction between Se and AC.

The BET test results (Fig. 2c and d, Fig. S4 and Table 1, Table S1) show that the pore diameter of the AC is slightly reduced, the specific surface area is reduced from 1892 m^2 g^{-1} to 1074 m^2 g^{-1} and the pore volume is reduced from 0.27 cm^3 g^{-1} to 0.20 cm^3 g^{-1} after the infiltration of Se into AC to form AC-Se composite. This indicates that the process of Se infiltration has little effect on the pore structure of AC, thus it has little effect on the capacitance characteristics of AC.

The interaction between Se and AC matrix in AC-Se-10 was examined by XPS measurements. In Fig. 3a, the C 1s spectrum of AC-Se-10 consists of four peaks, which correspond to C=C bonding (284.5 eV), C−C/C−Se bonding (285.3 eV), C−O bonding (286.4 eV), and O−C=O bonding (288.4 eV). The Se 3d XPS spectrum was deconvoluted into three sub peaks (Fig. 3b). The two peaks at around 56.2 and 55.4 eV are assigned to the 3d$_{3/2}$ and 3d$_{5/2}$ of elemental Se. The broad peak at around 58.9 eV is ascribed to the Se 3d electrons having strong interaction with AC host through C−Se or Se−O bonds [17,18].

Next, the LSECs asymmetric energy storage batteries have been assembled and tested for electrochemical performance. The comparison of cycle performance between several materials is shown in Fig. S5. It can be seen that compared with AC-Se composites, the cycle of AC is stable, but the capacity is lower, the capacity and cycle performance of Se are also poor. For AC-Se composites, as the Se content increases, the specific capacity gradually increases, but the capacity decay increases. The comprehensive performance of the AC-Se-10 is optimal, so it is selected for detailed study. The assembled LSECs have been subjected to CV and constant current charge and discharge measurement using AC or AC-Se-10 as a cathode material and prelithiated graphite as an anode material. The results are shown in Fig. 4. As shown in Fig. 4a, the CV curves of batteries based on the AC (LIC) and the AC-Se-10 (LSEC) show

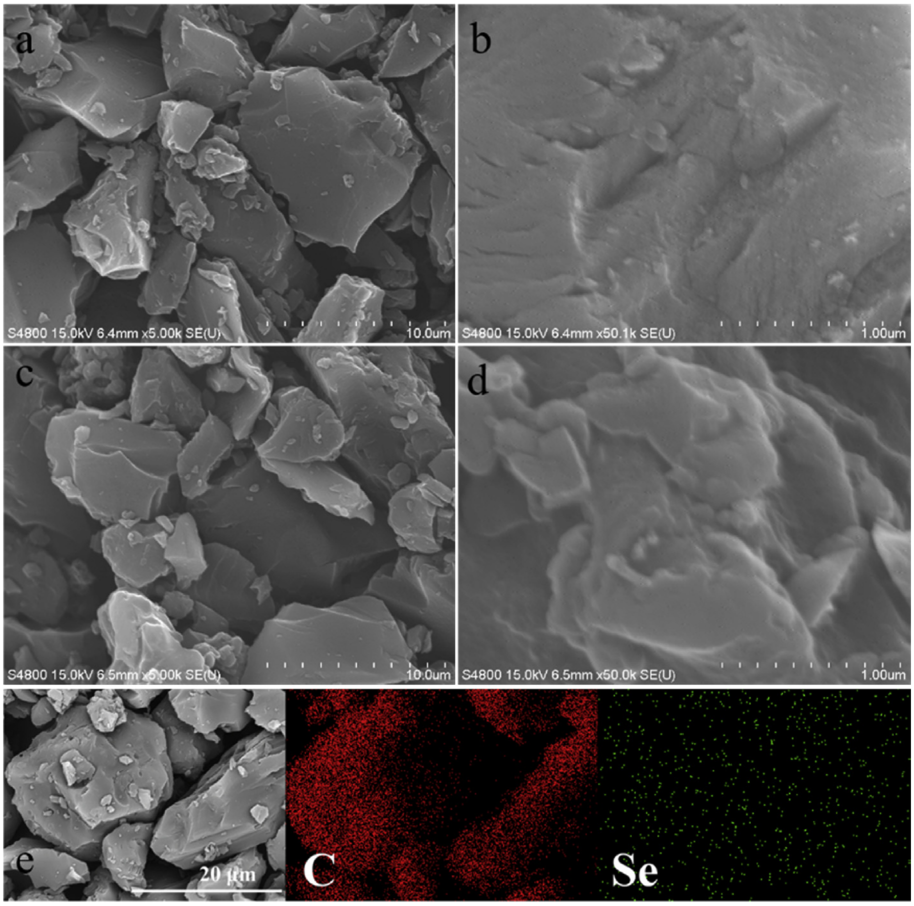

Fig. 1. The morphologies of the AC and AC-Se-10: (a, b) SEM images of the AC, (c, d) SEM images of the AC-Se-10, (e) element mapping of the AC-Se-10.

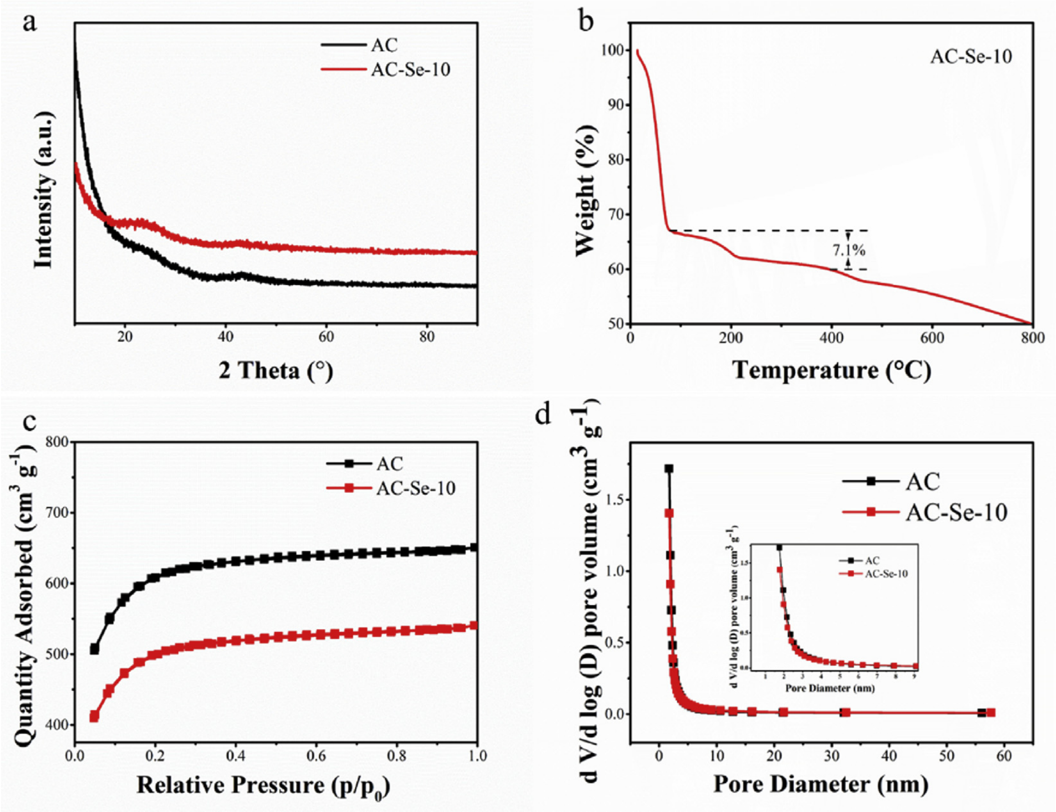

Fig. 2. Characterization of the AC and AC-Se-10 materials. (a) XRD of the AC and AC-Se-10, (b) TG curve of the AC-Se-10, (c, d) Nitrogen adsorption-desorption isotherms curves and the corresponding BJH data of the AC and AC-Se-10.

Table 1
The corresponding specific surface area and pore volume of the AC and AC-Se-10.

	BET (m^2 g^{-1})	Volume of pores (cm^3 g^{-1})
AC	1892	0.27
AC-Se-10	1543	0.22

quasi-rectangular shapes, indicating that they all exhibit electrical double layer capacitance behavior. Compared with the battery based on AC, a pair of redox peaks, namely the Faraday reaction of Se, is also observed in the CV curve of the battery based on AC-Se-10, which indicates that AC-Se-10 shows a pseudocapacitive performance. Therefore, these batteries based on AC-Se-10 belong to an asymmetric energy storage system, and work through a hybrid charge-storage mechanism which can be attributed to the different characteristics of AC and Se [17]. Interestingly, the broad reduction peak splits into two peaks at ~2.0 and ~1.6 V and the broad oxidation peak splits into two peaks at ~2.2 and ~2.3 V during the scanning, respectively. According to the previously reported Li—Se battery reaction mechanism, the two reduction peaks can be attributed to the reduction of elemental Se to soluble polyselenides and then to the insoluble Li_2Se_2 and Li_2Se, respectively [19,20]. The different lithiation plateaus can be ascribed to different interaction strengths exhibited by different Se molecules with nanopores [21].

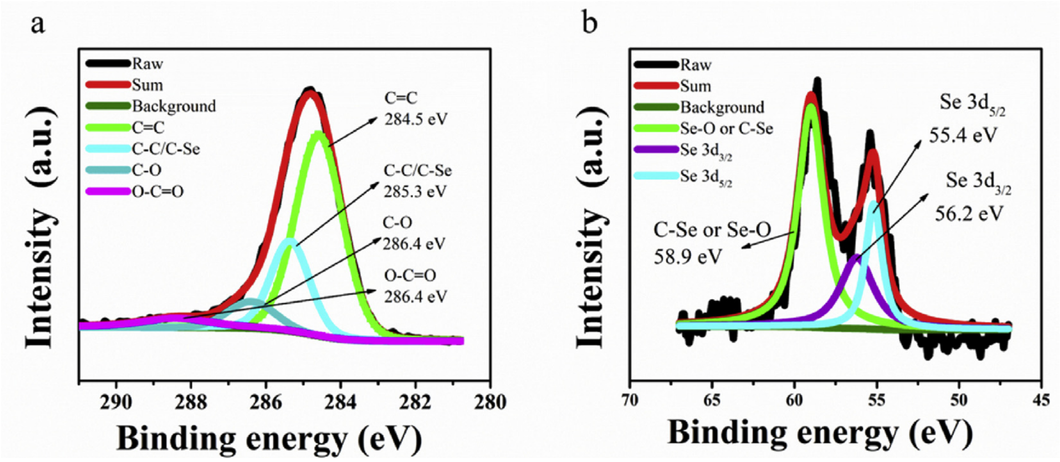

Fig. 3. XPS spectra of the AC-Se-10: (a) C 1s and (b) Se 3d.

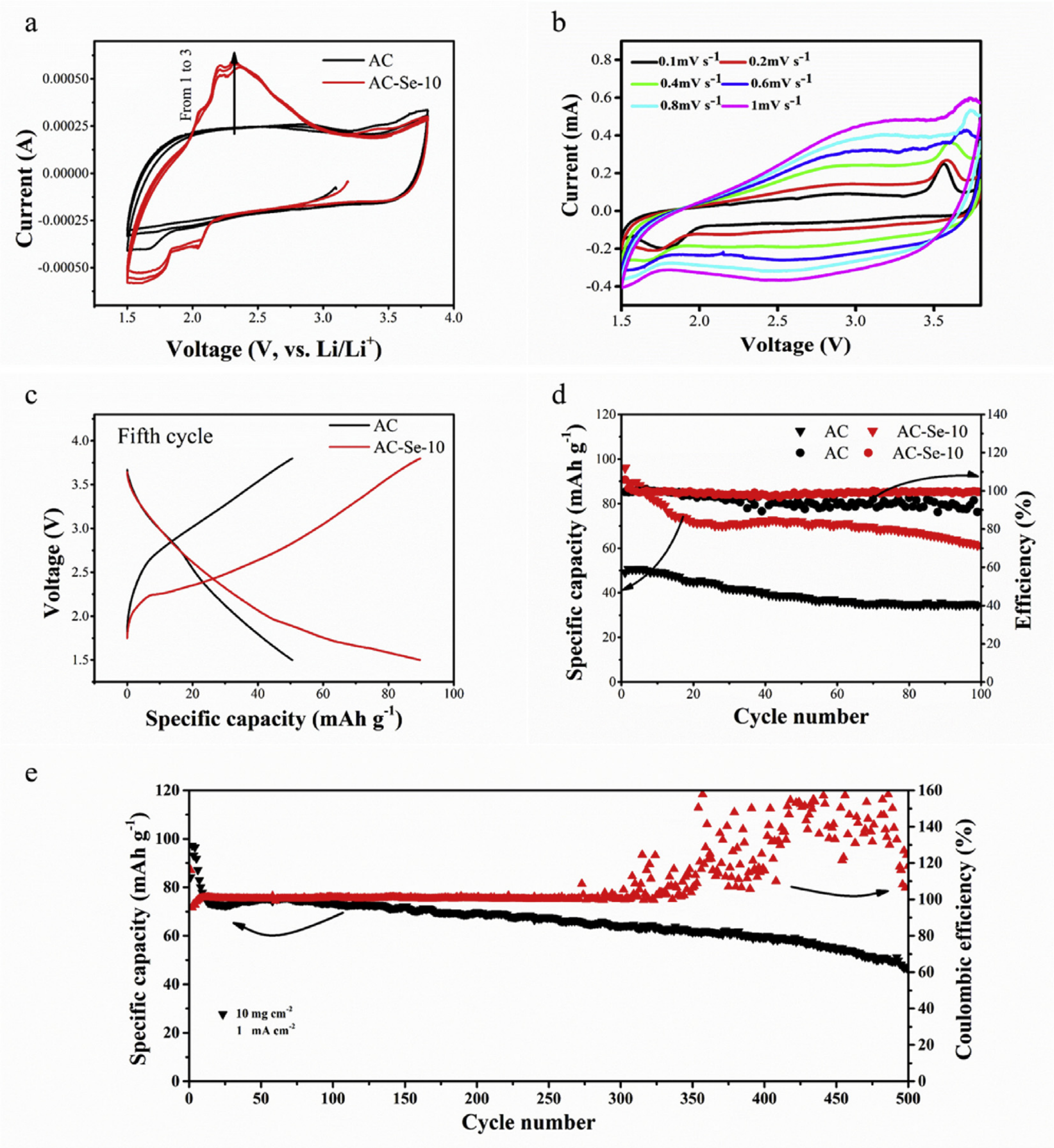

Fig. 4. Electrochemical performance of the AC-Se-10 (LSEC) and AC (LIC) as the cathode material and prelithiated graphite as the anode material in the voltage range of 1.5–3.8 V versus Li/Li$^+$. (a) the CV of the LSEC and LIC at 0.1 mV s^{-1}, (b) the CV of the LSEC at different scan rates from 0.1 mV s^{-1} to 1.0 mV s^{-1}, (c) the fifth charge-discharge curve of the LSEC and LIC at the current of 0.5 mA cm^{-2}, (d) the cycle performance of the LSEC and LIC at the current of 0.5 mA cm^{-2}, (e) the long cycle performance of the LSEC at the current of 1 mA cm^{-2} (The specific capacity is calculated according to the mass of AC-Se composite).

The two oxidation peaks observed during the anode scanning can be attributed to the delithiation, suggesting that Li_2Se_2 and Li_2Se can return to polyselenides and eventually return to Se. Therefore, during the cycle, the polyselenides can be finally converted into Se, which maintains high reversibility and high utilization rate of Se. The shapes of the CV curves are close to each other and There is no apparent change in the position of the CV peak after the first three cycles, demonstrating that the battery based on the AC-Se-10 composite cathode may have similar reversibility during the scanning.

From Fig. 4b, we can see that the battery exhibits polarization with increased scanning speed. However, except that the two oxidation peaks gradually coincide with the increasing of the scan rate, the two reduction peaks are well maintained even at high scan rate, indicating that the LSECs exhibit superior rate performance and superior reversibility. Fig. 4c is the charge and discharge curves for the LSECs and the LICs in the voltage range of 1.5–3.8 V. It can be seen that the charge and discharge curves of both the LSECs and the LICs have similar platforms when the cycling is stabilized at 0.5 mA cm^{-2} until the fifth cycle. The capacities are about 90 mAh g^{-1} and 50 mAh g^{-1}, respectively, and the LSECs show a much higher capacity than the LICs. Fig. 4d presents the charge and discharge cycle performance of the LSECs and the LICs at a current density of 0.5 mA cm^{-2}. As indicated, the LSECs show higher capacity and higher Coulomb efficiency than the LICs. After 100 cycles, the capacity of LSECs remains at around 70 mAh g^{-1}. In addition, the Coulomb efficiency of LSECs is close to 100%, indicating that the LSECs have excellent reversibility. Fig. 4e shows the long cycle performance of the LSECs at a current density of 1 mA cm^{-2}. It can be seen that the LSECs has a good long cycle performance before 400 laps, however, the capacity decay is accelerated after 400 laps. It may be that after a long period of circulation, the AC physical confinement has not been able to properly limit the dissolution of Se. In subsequent studies, the AC may be modified or other porous materials having a stronger interaction with Se may be used as the substrate. The cycle performance of the LSECs under 55°Cis shown in Fig. S6. It can be seen that the LSECs also has excellent cycle performance under 55 °C. The electrochemical performance of the LSECs is compared with the corresponding literature, and the results are shown in Table S2. It can be seen that the LSECs has excellent electrochemical performance under high load compared with other work.

In order to understand the charge-storage mechanism of LSECs, further analysis has been performed according to the data of CV at different scan rates, and the results are shown in Fig. 5 (See the supporting information for specific principles). The cathodic current i of the CV curves (Fig. 4b) at the potential of 1.5, 2.0, 2.5 and 2.9 V is selected, and then log i is plotted against log υ, and the results are shown in Fig. 5a. It can be seen from the figure that at the four potentials of 1.5, 2.0, 2.5 and 2.9 V, the b values are 0.44, 0.58, 0.76, and 0.76, respectively, indicating that the LSECs have the diffusion-controlled reaction at the potential of 1.5 V and the LSECs have both the capacitive effect and the diffusion-controlled reaction at the potential of 2.0, 2.5 and 2.9 V. More specifically, when the potentials are 1.5 and 2.0 V, closing to the reduction peak potential of Se, the b values are 0.44 and 0.58, which are close to 0.5, indicating that the LSECs mainly undergo the diffusion-controlled redox reaction of Se. However, the values of b at a potential of 2.5 and 2.9 V are 0.76, which is close to 1.0, indicating that the surface capacitive reactions in LSECs increases [22–24].

The cathodic current i of the CV curves (Fig. 4b) at the potential of 2.0, 2.5 and 2.9 V is selected, and then $i/\upsilon^{1/2}$ is plotted against $\upsilon^{1/2}$, and the results are shown in Fig. 5b, c and Table 2. It can be seen that at the potentials of 2.0 V, which are close to the reduction peak potential of Se, the ratios of the diffusion-controlled reactions (0.1 mV s^{-1}) are 90.13%, indicating that the LSECs mainly undergo the diffusion-controlled redox reaction of Se. However, at a potential of 2.5 and 2.9 V, the ratios of the surface capacitive element and diffusion-controlled reactions (0.1 mV s^{-1}) are 35.29% and 64.71%, 36.73% and 63.27%, respectively, indicating that the surface capacitive reactions in LSECs increases [21–23].

To demonstrate the rate performance of LSEC, a series of electrodes were prepared, including a range of area load from ~5.5 mg cm^{-2} to ~ 10.0 mg cm^{-2}. The rate performance of LSECs was tested at the current from 0.5 to 50 mA cm^{-2}, and the results are shown in Fig. 6. As shown in Fig. 6, the LSEC has excellent rate performance, maintaining a capacity of ~22 mAh g^{-1} even at a high area load of ~5.5 mg cm^{-2} and a high current density of 20 mA cm^{-2}. When the current density is changed to 0.5 mA cm^{-2}, the capacity can be almost fully recovered.

In summary, the excellent electrochemical performance of LSECs may be due to two reasons. First of all, there is a large amount of AC in the AC-Se-10 composite, and its abundant pore structure can well inhibit the dissolution and shuttle of a small amount of Se during the cycling. Secondly, because of the high conductivity and high specific surface area of AC, as well as the high specific capacity, high density and high conductivity of Se, the immersion of Se in AC has little effect on its pore structure and conductivity. Therefore, the LSECs can simultaneously exhibit good surface capacitance and pseudocapacitance.

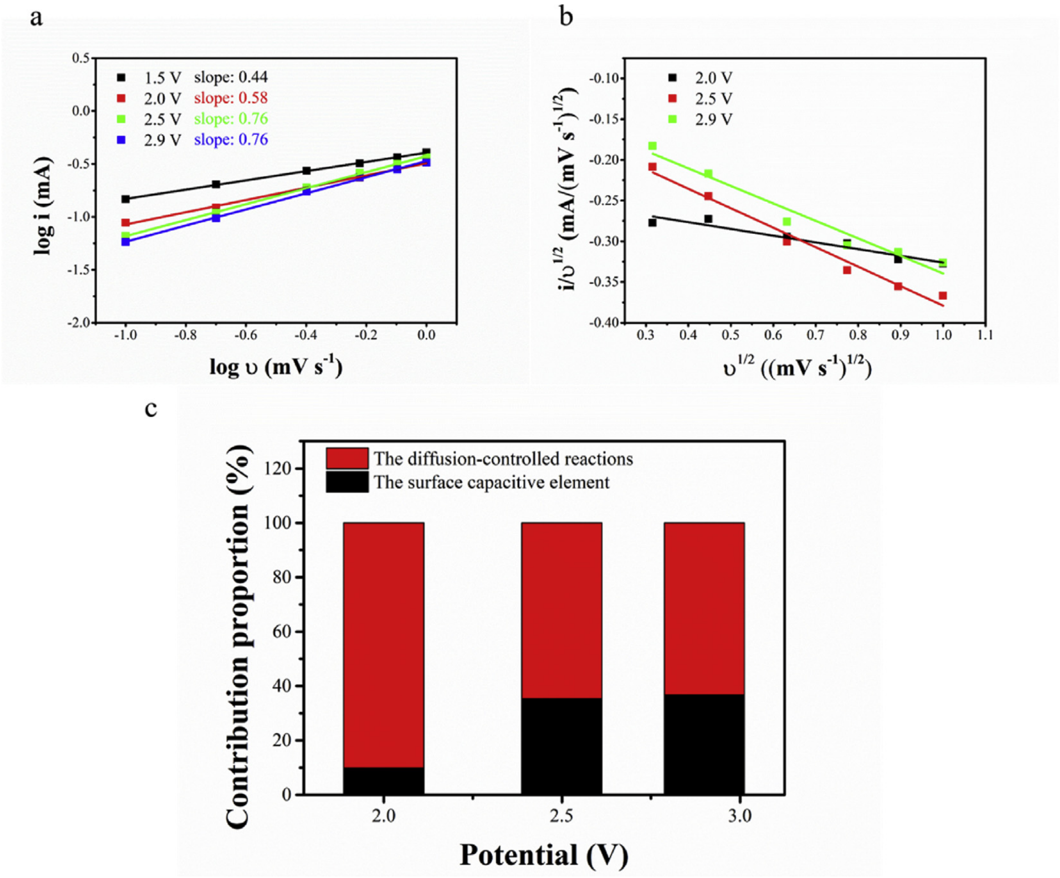

Fig. 5. Quantitative analysis of the storage mechanism of the LSECs. (a) the corresponding log i ~ log υ scatters and linear fitting of the CV curves (Fig. 4b) at the potential of 1.5, 2.0, 2.5 and 2.9 V, (b) the corresponding $i/\upsilon^{1/2}$ ~ $\upsilon^{1/2}$ scatters and linear fitting of the CV curves (Fig. 4b) at the potential of 2.0, 2.5 and 2.9 V. (c) The contribution proportion of surface capacitance and diffusion-controlled capacitance in the total charge storage of LSECs at different potential.

Table 2
The contribution proportion of surface capacitance and diffusion-controlled capacitance in the total charge storage of LSECs.

	Slope (k_1)	Intercept (k_2)	Ratio of the surface capacitive element ($k_1\upsilon$) (0.1 mV s^{-1})	Ratio of the diffusion-controlled reactions ($k_2\upsilon^{1/2}$) (0.1 mV s^{-1})
2.0 V	−0.083	−0.24	9.87%	90.13%
2.5 V	−0.24	−0.14	35.29%	64.71%
2.9 V	−0.22	−0.12	36.73%	63.27%

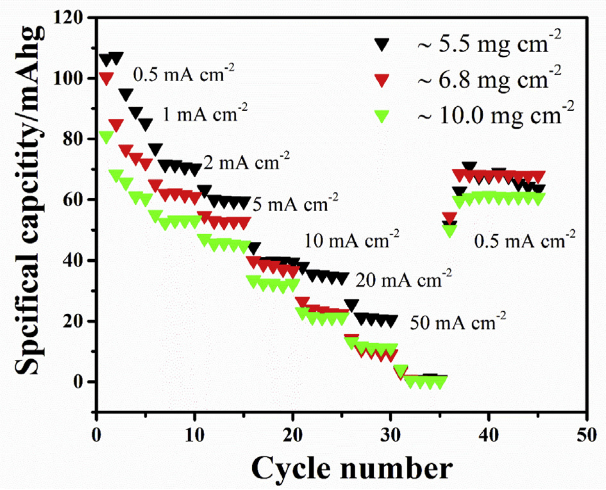

Fig. 6. The rate performance of LSECs at 0.5 mA cm^{-2}–50 mA cm^{-2}in region of 1.5–3.8 V.

4. Conclusions

We have successfully designed and fabricated a unique asymmetric energy storage system by using the AC-Se as a cathode material and the pre-lithiated graphite as an anode material. This asymmetric energy storage system has both the capacitive effect and the diffusion-controlled reaction. Therefore, it has both high energy density and power density, thus solves the problem of imbalance between the high energy and the low dynamics, and has great application potential. However, as the results presented in this paper, further researches are required. For example, a substrate with a higher specific capacitance can be used to carry Se, or an SSe_x compound with better kinetics can be used as a Faraday reaction-active material.

Author contribution

Yiyong Zhang and *Mingsheng Xu* conceived and designed the study. *Yiyong Zhang* and *Mingsheng Xu* performed the experiments. *Yiyong Zhang* and *Mingsheng Xu* wrote the paper. *Huaicong Yan, Qi Meng, Xue Li and Peng Dong* reviewed and edited the manuscript. The study was executed under the supervision of *Yingjie Zhang* and *Jinbao Zhao*. All authors read and approved the manuscript.

Conflict of interest

The authors declare that they have no known competing financial interests or personal relationships that could have appeared to influence the work reported in this paper.

Acknowledgments

We gratefully acknowledge the financial support of National Natural Science Foundation of China (Grant Nos. 21273185, 51604132 and 21321062). The authors also wish to express their thanks to Prof. D. W. Liao for his valuable suggestions.

Appendix A. Supplementary data

Supplementary data to this article can be found online at https://doi.org/10.1016/j.mtener.2019.100374.

References

[1] J.M. Tarascon, M. Armand, Issues and challenges facing rechargeable lithium batteries, Nature 414 (2001) 359–367.
[2] M. Armand, J.-M. Tarascon, Building better batteries, Nature 451 (2008) 652–657.
[3] M.S. Whittingham, Lithium batteries and cathode materials, Chem. Rev. 104 (2004) 4271–4301.
[4] S. Arico, P. Bruce, B. Scrosati, J.M. Tarascon, W.V. Schalkwijk, Nanostructured materials for advanced energy conversion and storage devices, Nat. Mater. 4 (2005) 366–377.
[5] M.V. Reddy, G.V. Subba Rao, B.V. Chowdari, Metal oxides and oxysalts as anode materials for Li ion batteries, Chem. Rev. 113 (2013) 5364–5457.
[6] D. McCloskey, J. Phys, Expanding the ragone plot: pushing the limits of energy storage, Chem. Lett. 6 (2015) 3592–3593.
[7] J. Lu, Z. Chen, Z. Ma, F. Pan, L.A. Curtiss, K. Amine, The role of nanotechnology in the development of battery materials for electric vehicles, Nat. Nanotechnol. 11 (2016) 1031–1038.
[8] B. Li, F. Dai, Q. Xiao, L. Yang, J. Shen, C. Zhang, M. Cai, Nitrogen-doped activated carbon for a high energy hybrid supercapacitor, Energy Environ. Sci. 9 (2016) 102–106.
[9] K. Chan, H. Peng, G. Liu, K. Mcilwrath, X.F. Zhang, R.A. Huggins, Y. Cui, High-performance lithium battery anodes using silicon nanowires, Nat. Nanotechnol. 3 (2008) 31–35.
[10] Y. Zhang, L. Wang, Z. Guo, Y. Xu, Y. Wang, H. Peng, High performance lithium-air battery with a coaxial-fiber architecture, Angew. Chem. 128 (2016) 4563–4567.
[11] Y. Yang, G. Zheng, Y. Cui, Nanostructured sulfur cathodes, Chem. Soc. Rev. 42 (2013) 3018–3032.
[12] M.D. Slater, D. Kim, E. Lee, C.S. Johnson, Sodium-ion batteries, Adv. Funct. Mater. 23 (2013) 947–958.
[13] L. Zhou, F. Xiong, S. Tan, Q. An, Z. Wang, W. Yang, Z. Tao, Y. Yao, J. Chen, L. Mai, Nickel-iron bimetallic diselenides with enhanced kinetics for high-capacity and long-life magnesium batteries, Nano Energy 54 (2018) 360–366.
[14] K. Naoi, S. Ishimoto, J. Miyamoto, W. Naoi, Second generation 'nanohybrid supercapacitor': evolution of capacitive energy storage devices, Energy Environ. Sci. 5 (2012) 9363–9373.
[15] J.-H. Kim, J.-S. Kim, Y.-G. Lim, J.-G. Lee, Y.-J. Kim, Effect of carbon types on the electrochemical properties of negative electrodes for Li-ion capacitors, J. Power Sources 196 (2011) 10490–10495.
[16] J.H. Lee, W.H. Shin, M.-H. Ryou, J.K. Jin, J. Kim, J.W. Choi, Functionalized graphene for high performance lithium ion capacitors, ChemSusChem 5 (2012) 2328–2333.
[17] M.H. Kim, H.K. Kim, K. Xi, R.V. Kumar, D.S. Jung, K.B. Kim, K.C. Roh, Lithium-sulfur capacitors, ACS Appl. Mater. Interfaces 10 (2018) 6199–6206.
[18] J. Yang, H. Gao, D. Ma, J. Zou, Z. Lin, X. Kang, S. Chen, High-performance Li-Se battery cathode based on $CoSe_2$-porous carbon composites, Electrochim. Acta 264 (2018) 341–349.
[19] Y. Cui, A. Abouimrane, J. Lu, T. Bolin, Y. Ren, W. Weng, C. Sun, V. Maroni, S. Heald, K. Amine, (De)Lithiation mechanism of Li/SeS_x (x=0-7) batteries determined by in situ synchrotron X-ray diffraction and X-ray absorption spectroscopy, J. Am. Chem. Soc. 135 (2013) 8047–8056.
[20] Y. Qu, Z. Zhang, S. Jiang, X. Wang, Y. Lai, Y. Liu, J. Li, Confining selenium in nitrogen-containing hierarchical porous carbon for high-rate rechargeable lithium-selenium batteries, J. Mater. Chem. A. 2 (2014) 12255–12261.
[21] H. Ye, Y.-X. Yin, S.-F. Zhang, Y.-G. Guo, Advanced Se-C nanocomposites: a bifunctional electrode material for both Li-Se and Li-ion batteries, J. Mater. Chem. 2 (2014) 13293–13298.
[22] E. Lim, C. Jo, M.S. Kim, M.-H. Kim, J. Chun, H. Kim, J. Park, K.C. Roh, K. Kang, S. Yoon, J. Lee, High-performance sodiumion hybrid supercapacitor based on Nb_2O_5@carbon core-shell nanoparticles and reduced graphene oxide nanocomposites, Adv. Funct. Mater. 26 (2016) 3711–3719.
[23] J. Duay, S.A. Sherrill, Z. Gui, E. Gillette, S.B. Lee, Self-limiting electrodeposition of hierarchical MnO_2 and $M(OH)_2/MnO_2$ nanofibril/nanowires: mechanism and supercapacitor properties, ACS Nano 7 (2013) 1200–1214.
[24] S. Wang, J. Polleux, J. Lim, B. Dunn, Pseudocapacitive contributions to electrochemical energy storage in TiO_2 (anatase) nanoparticles, J. Phys. Chem. C 111 (2007) 14925–14931.